New Semiempirical Formula for Evaluating the Equilibrium Scour Depth at Bridge Piers

A NEW SEMI-EMPIRICAL FORMULA FOR EVALUATING THE EQUILIBRIUM SCOUR DEPTH AT BRIDGE PIERS

Francesco Giordana[1], Davide Vettori[2], Federico Mana[3], Davide Demichele[4], and Costantino Manes[5]

[1]PhD Student, Dept. of Environment, Land and Infrastructure Engineering, Politecnico di Torino, Corso Duca degli Abruzzi 24, 10129 Torino, Italy (corresponding author). Email: francesco.giordana@polito.it

[2]Lecturer, James Watt School of Engineering, University of Glasgow, Glasgow, G12 8QQ, Scotland. Email: davide.vettori@glasgow.ac.uk

[3]Engineer, MM Construction Srl, 12038 Savigliano, Italy. Email: federico.mana.95@gmail.com

[4]PhD Student, Dept. of Environment, Land and Infrastructure Engineering, Politecnico di Torino, Corso Duca degli Abruzzi 24, 10129 Torino, Italy. Email: davide.demichele@polito.it

[5]Associate Professor, Dept. of Environment, Land and Infrastructure Engineering, Politecnico di Torino, Corso Duca degli Abruzzi 24, 10129 Torino, Italy. Email: costantino.manes@polito.it

ABSTRACT

Estimating the equilibrium scour depth (y_{se}) at bridge piers is essential for both bridge foundation design and flood risk assessment. Traditional methods typically rely on empirical formulas derived from data-fitting procedures, which often result in significant overestimations of the local scour phenomenon. While such conservative predictions may be acceptable for design purposes, they are less suitable for accurate risk evaluation. In this paper, we propose a new formula for predicting y_{se}, grounded in a theoretical framework previously developed by one of the authors. This foundation is enhanced with empirically derived functions, obtained from laboratory data, to account for complex phenomena that remain difficult to capture theoretically, such as sediment

non-uniformity. We demonstrate that the resulting semi-empirical formula consistently outperforms five of the most widely used local scour methods in the literature. Predictive accuracy is evaluated through four different performance metrics, using over 600 laboratory data and some selected field data whereby the formula could be confidently applied. The proposed approach provides unbiased estimates and avoids the systematic overestimations that characterize the reference methods, thus making it particularly suitable for risk assessment applications. Furthermore, the potential extension of the model to bridge design is discussed, proposing the introduction of an appropriate safety factor. Finally, we discuss the limitations of the proposed model and outline potential directions for future improvements.

Author keywords: Bridge piers; Local scour; Equilibrium scour depth; Non-uniform sediments; Risk assessment.

INTRODUCTION

Local scouring at piers is considered a major cause of bridge-failure and is a primary concern for transportation agencies and local authorities worldwide (Wardhana and Hadipriono 2003; Maddison 2012). It is widely accepted that the initiation and evolution of pier local-scour is primarily driven by the erosive power of the (so-called) horseshoe vortex that develops at the interface between the erodible bed and the base of the pier (Melville and Coleman 2000; Lee and Sturm 2009; Ettema et al. 2011). As the scour hole deepens, the erosive capacity of the vortex gradually decreases until a condition of equilibrium is reached (Melville and Chiew 1999). Accurately estimating the so-called equilibrium scour depth (y_{se}) is essential for bridge design and flood-related risk assessments, hence significant research efforts have been dedicated to developing formulas to predict y_{se}, mainly adopting an empirical approach. There is general consensus that, for cylindrical piers with circular cross-section under steady flow conditions, the non-dimensional scour depth of equilibrium, expressed as y_{se}/a (where a represents the pier diameter), depends on the following non-dimensional parameters:

$$\frac{y_{se}}{a} = f\left(\frac{h}{a}, \frac{a}{d}, \frac{U}{U_c}, Fr_a, Re_a, \frac{\rho_s}{\rho}, \sigma_g\right), \tag{1}$$

where, f is an unknown functional relation, h is the flow depth, d the characteristic sediment diameter (i.e. d_{50}), U the cross-sectional average velocity of the flow upstream of the pier, U_c the sediment critical velocity, $Fr_a = U/\sqrt{ga}$ the pier Froude number, g the gravitational acceleration, $Re_a = Ua/\nu$ the pier Reynolds number, ν the fluid kinematic viscosity, ρ_s and ρ the sediment and fluid densities, and σ_g the geometric standard deviation of the sediment particle size distribution (Ettema et al. 1998; Ettema et al. 2006; Ettema et al. 2011).

Most of the currently available formulas for predicting y_{se}/a (e.g. Froelich 1988; Melville 1997; Richardson and Davis 2001; Sheppard and Miller 2006; Sheppard et al. 2014) were derived from data-fitting procedures used on (mainly) laboratory data, with the aim of establishing relations between y_{se}/a and each individual governing parameter reported on the right-hand side of Eq. 1 (or other different parameters depending on how dimensional analysis was carried out in different studies). However, such empirical approaches may be affected by scale issues, which can arise from the difficulties in simultaneously satisfying all the similarity conditions between laboratory and field scales. For example, matching both Fr_a and Re_a is generally not feasible without introducing a trade-off in model accuracy, as reproducing Fr_a of the prototype scale typically results in too low Re_a at the laboratory scale. In addition, these empirical formulas were developed to be quite conservative meaning that, very often, they provide significant overestimations of y_{se} when applied to both field and laboratory data, leading to a poor agreement between measured and estimated values of y_{se}. While such conservative predictions may be acceptable for design purposes, they are less suited for risk assessment procedures. In engineering practice, when over-conservative formulas for estimating local scour are applied in bridge risk assessments, they often classify most or all bridges as high-risk. This limits the ability to rank structures accurately, making it difficult for asset owners to prioritize, and hence optimize, resources dedicated to maintenance and improved flood-resilience efforts.

Manes and Brocchini (2015), hereafter referred to as MB15, employed a physically grounded framework based on turbulence phenomenology to derive scaling relations between y_{se}/a and some of the governing parameters listed in Eq. 1 (i.e. $a/d, U/U_c, Fr_a, \rho_s/\rho$). The scaling

relations proposed by MB15 were developed for uniform sediments in both clear-water and live-bed conditions, under the hypotheses of large values of Re_a and relative coarseness a/d. As this approach directly stems from theoretical considerations rather than from physical modelling or empirical data-fitting, it is virtually free from scale-effects. Coscarella et al. (2020), hereafter referred to as CGM20, extended the applicability of MB15 by accounting for Re_a-effects and low relative coarseness (i.e. low a/d) in clear-water conditions. Moreover, CGM20 discusses the role played by h/a, deeming it as negligible.

The aim of the present study is to build upon the theoretical foundations laid out by MB15 and CGM20 to: (i) identify empirical functions accounting for the effects of low a/d-values in live-bed conditions and of non-uniform sediments (as quantified by σ_g) on scour; (ii) retrieve a semi-empirical formula accounting for all the relevant non-dimensional parameters appearing in Eq. 1; and (iii) demonstrate that the retrieved semi-empirical formula outperforms fully-empirical methods available from the literature when predicting local scour. Such a formula is developed to reproduce experimental measurements without overestimation biases and hence it targets risk-assessment applications. We will demonstrate, though, that when appropriate safety factors are employed, it can be used also for design purposes.

In what follows, we first review the formulations proposed by MB15 and CGM20. We then extend the latter to account for low a/d values under live-bed conditions and the influence of non-uniform sediments. The performance of the newly proposed formula is subsequently evaluated against the most widely used empirical formulas from the literature, using both laboratory and field experimental data. Finally, we provide a comprehensive discussion of the proposed formula, highlighting its limitations and outlining potential research-avenues for further enhancing its predictive capability.

SUMMARY OF MB15 AND CGM20

In clear-water conditions ($0.5 \leq U/U_c \leq 1$), equilibrium occurs when the shear stress within the scour hole approaches the critical shear stress for the sediments (Ettema et al. 2011) and y_{se} can be either defined as the maximum scour depth reached at a given finite time (Melville and

Chiew 1999) or asymptotically for time approaching infinity (Sheppard et al. 2004; Lança et al. 2013). This condition, applied to the deepest point of the scour hole, is expressed by the relation $\tau = \tau_c \sim (\rho_s - \rho)gd$, where τ is the bed shear stress and τ_c is the critical shear stress of the sediments. Building on a series of hypotheses and employing Kolmogorov's theory to characterize turbulence within the scour hole, MB15 refined the equilibrium condition to derive the following scaling relationship for y_{se}:

$$\frac{y_{se}g}{U^2} \sim \left(\frac{\rho}{\rho_s - \rho}\right)(C_d)^{2/3}\left(\frac{a}{d}\right)^{2/3}, \tag{2}$$

where C_d is the drag coefficient of the part of the pier exposed to scouring. There are four assumptions underpinning Eq. 2: (i) the flow within the scour hole is in the fully rough regime; (ii) the large-eddies generated within the scour hole are comparable in size to y_{se}; (iii) the mean sediment diameter d belongs to the inertial range of turbulence, namely $\eta << d << y_{se}$ (where η is the Kolmogorov's length scale); and (iv) the power of the horseshoe vortex (i.e. turbulent kinetic energy per unit mass and unit time required to feed the horseshoe vortex) can be estimated from the product of the drag force acting on the part of the cylinder exposed to scour and the velocity used to estimate such a drag force. Due to these assumptions and the data employed for its validation, Eq. 2 is applicable exclusively to flow regimes characterized by large values of Re_a where viscosity effects are negligible (i.e. $d/\eta > 5$) and deep scour holes, i.e. $d << y_{se}$. MB15 report that if a is used as an a-priori estimation of y_{se} (i.e. its order of magnitude), experimental observations show that the proposed scaling works very well for $a/d > 20$.

In live-bed conditions, equilibrium is determined by a mass balance of sediments moving in and out of the scour hole (Melville 1984), with y_{se} defined as the time average of the maximum scour depth, which fluctuates over time due to the passage of bed forms. Mathematically, this condition can be expressed by the relation $Q_{in} = Q_{out}$, where Q_{in} and Q_{out} are the average fluxes of sediment entering and exiting the scour hole, respectively at equilibrium conditions. MB15 assumed that Q_{in} is predominantly in the form of bed load, hence it can be estimated as a function of U/U_c.

Then, by applying the same set of hypotheses as used for the analysis in clear-water conditions, they obtained the following live-bed scour function S_e:

$$S_e = \frac{\frac{y_{se} g}{U^2}}{\frac{\rho}{\rho_s - \rho} (C_d)^{2/3} \left(\frac{a}{d}\right)^{2/3}} = \Phi\left(\frac{U}{U_c}\right), \tag{3}$$

where the flow intensity function Φ was found empirically. The results were satisfactory because the scour function S_e, when plotted against U/U_c, allowed for an excellent data-collapse, except for data points with low relative coarseness, i.e. $a/d < 20$ as observed for clear-water conditions. Manipulating Eq. 3, MB15 obtained a formula for y_{se} normalized by the pier diameter a, i.e.

$$\frac{y_{se}}{a} \sim \Phi\left(\frac{U}{U_c}\right) (Fr_a)^2 \left(\frac{\rho}{\rho_s - \rho}\right) (C_d)^{2/3} \left(\frac{a}{d}\right)^{2/3}, \tag{4}$$

with $\Phi(U/U_c) = 1$ for $U/U_c \leq 1$. Eq. 4 establishes a relation between y_{se}/a and all the governing non-dimensional parameters reported in Eq. 1, except for h/a and Re_a. However, MB15 argued that, these two parameters may be partly accounted for through their indirect effects on C_d.

CGM20 revisited the work of MB15 to broaden its applicability in clear-water conditions by addressing viscous and low relative-coarseness effects on local scouring. Coupling theoretical and empirical arguments, they derived two corrective functions, $f_1(d/\eta)$ and $f_2(a/d)$. The corrective function $f_1(d/\eta)$, which accounts for viscous effects on y_{se}, is defined as

$$f_1\left(\frac{d}{\eta}\right) = F_1 \left\{0.22 \left(\frac{d}{\eta}\right)^{-0.6} + 0.12 \exp\left[-17.77 \left(\frac{d}{\eta}\right)^{-0.6}\right]\right\}, \tag{5}$$

where $\eta = (\nu^3 a/(C_d U^3))^{1/4}$ is the Kolmogorov's length scale and F_1 a coefficient that compensates for the different definitions of equilibrium in clear-water conditions ($F_1 = 28$ if y_{se} is defined at a given finite time or $F_1 = 22$ if y_{se} is defined asymptotically). Eq. 5 retains the mathematical formulation proposed by Brownlie (1981) to fit the experimental data from Shields (1936) and describes the behavior of a non-dimensional critical shear stress τ_c (i.e. the so-called Shields parameter) as a function of d/η, used as a surrogate of the roughness Reynolds number. On the

other hand, the corrective function $f_2(a/d)$ accounts for low a/d effects and is defined as

$$f_2\left(\frac{a}{d}\right) = 1 + 6\exp\left(-0.18\frac{a}{d}\right). \tag{6}$$

Physically, Eq. 6 expresses that if $a/d < 20$, τ_c within the scour hole increases if a/d decreases (and consequently y_{se} decreases, see Eq. 7). CGM20 indicates that this is in line with the standard theory of incipient sediment motion where the low relative submergence for uniform open channel flows (i.e. h/d) plays the same role as a/d in the game of clear-water scouring around piers. Despite these encouraging results, CGM20 warns that low values of a/d are often encountered for large sediment diameters d and hence very permeable beds. Unfortunately permeability effects are known to affect τ (Manes et al. 2011; Manes et al. 2012) and possibly τ_c but these effects are not accounted for in the theoretical approach developed by MB15 and CGM20. On top of this, CGM20 also warns that low values of a/d can be encountered for relatively small scour holes whereby the horseshoe vortex is not fully buried, which is an important hypothesis underpinning the MB15 approach. Hence, it was concluded that f_2 may incorporate the lumped effect of several causes.

By integrating the work of MB15 with these new insights, CGM20 proposed an updated formula for modeling local scouring in clear-water conditions with uniform sediments, i.e.

$$y_{se} = \frac{\frac{\rho}{\rho_s-\rho}\frac{U^2}{g}(C_d)^{2/3}\left(\frac{a}{d}\right)^{2/3}}{f_1\left(\frac{d}{\eta}\right)f_2\left(\frac{a}{d}\right)}, \tag{7}$$

where $f_1(d/\eta)$ and $f_2(a/d)$ are defined in Eq. 5 and Eq. 6 respectively.

EXTENSION OF CGM20 TO LIVE-BED CONDITIONS

According to MB15, in live-bed conditions, y_{se} can be related to a scour function S_e, which resembles a Shields mobility parameter and is dependent on the flow intensity U/U_c through a flow intensity function Φ (see Eq. 3). The function $\Phi(U/U_c)$ is here refined using a slightly larger dataset compared to MB15, encompassing a total of 207 laboratory experiments conducted in live-bed conditions with water flowing over uniform sediments and impinging on a circular

pier. This dataset (see Table 1) was extracted from the works of Shen et al. (1969), Chee (1982), Chiew (1984), and Sheppard and Miller (2006). There are two primary differences between the present dataset and that used in MB15: (i) 13 data points characterized by $U/U_c < 1$ were excluded (see Fig. 6 in MB15) to ensure consistency with the definition of live-bed conditions; and (ii) 54 additional measurements from Shen et al. (1969) and Chee (1982) were incorporated to expand the dataset and strengthen the validation of $\Phi(U/U_c)$. All data considered in this analysis refer to the time-averaged maximum scour depth, thereby the transient effects caused by migrating bedforms are filtered out, consistently with the definition of equilibrium in live-bed conditions. Throughout the paper, we adopted constant values for fluid and sediment densities (ρ = 1000 kg m^{-3} and ρ_s = 2650 kg m^{-3}, respectively), assumed C_d = 1.2 for circular piers, and used as sediment critical velocity U_c the values reported in the relevant references (see Table 1).

When S_e is plotted versus U/U_c (see Fig. 1a) most of the experimental data nicely collapse on a curve described by the following flow intensity function:

$$\Phi\left(\frac{U}{U_c}\right) = \beta\left(\frac{U}{U_c}\right)^{\gamma}, \tag{8}$$

with $\beta = 0.41$ and $\gamma = -1.75$. Because of the modified dataset considered herein, these values slightly differ from those reported by MB15 (i.e. 0.47 and -1.89, respectively).

MB15 observed that the data points which most deviate from Eq. 8 (i.e. the black markers) are characterized by $a/d < 20$, as observed by CGM20 for clear-water conditions. To compensate for the effects of low relative coarseness in clear-water conditions, CGM20 proposed to use the corrective function $f_2(a/d)$ (see Eq. 6). Herein, we propose to use the same approach and include $f_2(a/d)$ in the formulation of S_e to develop a corrected live-bed scour function $S_e{}'$, yielding:

$$S_e{}' = \frac{\frac{y_{se}g}{U^2} f_2\left(\frac{a}{d}\right)}{\frac{\rho}{\rho_s-\rho}\left(C_d\right)^{2/3}\left(\frac{a}{d}\right)^{2/3}} = \Phi\left(\frac{U}{U_c}\right). \tag{9}$$

In Fig. 1b, the corrected scour function $S_e{}'$ is plotted versus U/U_c. Interestingly, the introduction of $f_2(a/d)$, which CGM20 calibrated exclusively using clear-water data, results in a much better

alignment also of the live-bed data, independently of the relative coarseness. When interpreting this result, it is worth noting that the live-bed data with low relative coarseness included in the dataset are limited to $U/U_c = 1.2 - 1.8$ (that is, a narrow range just above the transition from clear-water to live-bed). Therefore, $f_2(a/d)$ should be checked, in future experimental studies, for larger flow intensities U/U_c.

It should be noted that the corrective function $f_1(d/\eta)$ (see Eq. 5), which accounts for viscous effects, is not included in our live-bed scour framework. This is because the equilibrium scour depth in live-bed conditions is dictated by the balance of bed-load sediment fluxes going in and out of the scour hole. Classical bed-load transport formulas (e.g. Meyer-Peter and Müller 1948) relate to the excess shear with respect to a non-dimensional critical shear stress, which is always assumed to be constant, i.e. independent of viscous effects. Consistently with classical bed-load formulations, here, we make the same assumption.

NON-UNIFORM SEDIMENTS EFFECTS

Previous studies have shown that sediment non-uniformity can significantly impact local scouring, often resulting in a considerably lower y_{se} compared to uniform sediments (see e.g. Raudkivi and Ettema 1983). Such a reduction is mainly attributed to the effect of armoring, with the flow selectively removing from the scour hole the finer portion of the sediment mixture and leading to the creation of a protective layer of coarser particles. This armored layer limits sediment transport by shielding the finer particles, preventing their entrainment, and reducing the overall amount of eroded material, thereby decreasing y_{se} (Chiew 1991). The process becomes more pronounced as sediment non-uniformity increases (Ettema 1980). The degree of sediment gradation is usually quantified by the geometric standard deviation of the particle size distribution σ_g. Given that the sediment size distribution in rivers often follows the log-normal probability distribution (Dey 2014), σ_g can be defined as the ratio of the sediment diameters exceeding 84% and 50% of the bed material, respectively, i.e., $\sigma_g = d_{84}/d_{50}$. The threshold between uniform and non-uniform sediments is commonly set at $\sigma_g = 1.5$ (Chiew 1984), with higher degrees of sediment gradation indicating non-uniform conditions. The analysis presented hereafter aims to develop a model ca-

pable of efficiently estimating y_{se} for high degrees of sediment gradation, first in clear-water and then in live-bed conditions.

Clear-water conditions

In clear-water conditions, the rate of sediment supply into the scour hole is zero. As a result, the non-uniform sediment bed undergoes a gradation process due to the erosion of the finer fraction caused by the increased bed shear stress until it is fully armored (Chiew 1991). Thus, sediment gradation influences both the scaling of the flow resistance (i.e. τ) and the initiation of sediment motion (i.e. τ_c). Concerning the flow resistance, Gioia and Bombardelli (2001) proposed a model that directly relates it to the statistical distribution of roughness element sizes. In contrast, classical formulas (e.g. Strickler's formula) relate resistance to the size of the coarser sediment fraction, assuming that the largest particles dictate the flow behavior. As for the initiation of sediment motion, Parker et al. (1982) illustrated a slight increase in the critical shear stress for a sediment mixture as the grains become coarser and related this tendency to hiding-exposure effects.

Given the complexities involved in theoretically modeling the effects of sediment gradation on τ and τ_c separately, we account for their combined action on y_{se}, through an empirical sediment gradation function $f_3(\sigma_g)$ that fits the available experimental data. The function $f_3(\sigma_g)$ is defined from the scour formulation proposed by CGM20 (see Eq. 7), rearranging it into a clear-water scour function $S_{e,CW}$, as follows:

$$S_{e,CW} = \frac{\frac{y_{se}g}{U^2} f_1\left(\frac{d}{\eta}\right) f_2\left(\frac{a}{d}\right)}{\frac{\rho}{\rho_s-\rho}(C_d)^{2/3}\left(\frac{a}{d}\right)^{2/3}} = f_3(\sigma_g), \tag{10}$$

where the characteristic diameter for non-uniform sediments d coincides with d_{50} and f_3 must be found empirically. Towards this end, we employed a collection of data from the works of Ettema (1976), Molinas (2004), Sheppard et al. (2004), Raikar and Dey (2005) and Guo et al. (2012), which comprises 119 experiments conducted in clear-water conditions with non-uniform sediments characterized by values of σ_g up to 4.6 (see Table 1). The measurements extracted from Ettema (1976), Molinas (2004), Raikar and Dey (2005), and Guo et al. (2012) report values of scour

depths recorded at finite times while Sheppard et al. (2004), determined y_{se} by extrapolating the curve describing the temporal evolution of the maximum scour depth to an infinite time. Following CGM20, we assigned $F_1 = 28$ to the former group of data and $F_1 = 22$ to the latter. It is worth noting that a few experiments of Raikar and Dey (2005) were performed with a square pier and for these cases we assumed $C_d = 2$.

The experimental data plotted in Fig. 2 show the expected reduction in scour depth attributed to armoring effects, with $S_{e,CW}$ approaching 1 as $\sigma_g = 1$ and decreasing as σ_g increases. The observed trend suggests that a suitable fitting curve may be represented by a sigmoid function as follows:

$$f_3(\sigma_g) = \frac{1}{c_4 + \exp\left(\frac{\sigma_g - c_1}{c_2}\right)} + c_3, \tag{11}$$

where $c_1 = 2.21$, $c_2 = 0.17$, $c_3 = 0.15$ and $c_4 = 1.18$.

Eq. 11 effectively captures the overall trend of the experimental data. The parameters c_3 and c_4 were determined by imposing two boundary conditions: (i) when the sediment bed is uniform ($\sigma_g < 1.5$), $f_3(\sigma_g)$ tends to 1, so that Eq. 10 coincides with the formula for uniform sediments (Eq. 7); and (ii) as the degree of sediment gradation increases, the estimated scour depth progressively decreases due to armoring, reaching a maximum reduction of approximately 85%, following the corrective function proposed by Raudkivi (1986) (see Fig. 6 in the cited paper). Notably, there is a certain degree of uncertainty associated with this latter hypothesis, as the available experimental data for highly non-uniform sediments are limited, making precise quantification challenging. Nevertheless, Raudkivi (1986) provides the most reasonable indication of the expected maximum scour depth reduction. Moreover, the few data points with $\sigma_g > 3$, show an acceptable agreement with this assumption. Regarding the estimation of parameters c_1 and c_2, their values were obtained by applying a best-fit procedure, once the other two parameters were fixed.

Live-bed conditions

Chiew (1984) reported that the effect of sediment gradation on y_{se} in live-bed conditions appears to be negligible for $\sigma_g < 2$, implying that the scour depth can be reliably estimated from Eq. 9, as if sediments were uniform. It follows that only when the degree of sediment gradation increases ($\sigma_g \geq 2$), the occurrence of armoring alters the scour mechanism reducing the scour depth. For what concerns the flow intensity, it is important to note that when dealing with non-uniform sediments, U_c represents the critical velocity referred to d_{50} of the sediment mixture. When the flow can only erode the finer fraction (say $U/U_c \gtrsim 1$) and the supply of sediments cannot keep up with the material being entrained, armoring occurs, closely resembling what happens in clear-water conditions. Intuitively, as U/U_c increases, the intensified bed shear stress leads to the dislodgment of all sediment grains regardless of their size so much so armoring effects (or, more in general, non-uniform sediments effects) are expected to become negligible (Melville and Sutherland 1988). This intuitive reasoning is supported by Fig. 3a, which displays the corrected live-bed scour function for uniform sediments $S_e{}'$ (Eq. 9) plotted against U/U_c for all experiments performed in live-bed conditions. The 108 experimental data were extracted from Shen et al. (1969) and Chiew (1984), covering a range of σ_g up to 5.5 (see Table 1). Consistently with the approach adopted for uniform sediments, we considered only those data in which the equilibrium scour depth is defined as the time-averaged of the deepest measured scour depth (time averaging is used to filter out bed-form effects). The observed trend supports the idea that the effect of sediment gradation in live-bed conditions changes depending on flow intensity, with data showing two distinct behaviors. Once U/U_c exceeds a velocity threshold, experiments with non-uniform sediments show a good match with those with uniform sediments (data of experiments with uniform sediments are included in Fig. 3 for reference), nicely collapsing on the same curve. This confirms that the effect of sediment gradation becomes insignificant at high flow intensities. However, when U/U_c is below the threshold, data for non-uniform sediments tend to stratify horizontally at $S_e{}'$. The degree of stratification appears to depend on σ_g, with an observed reduction in scour depth with increasing sediment non-uniformity, consistently with the occurrence of armoring as observed in clear-water

conditions. We define this threshold as the critical armoring condition and characterize it using $U_{c,d_{84}}$, which is the critical velocity associated with d_{84}. We estimated it following a two-step procedure. First, we computed the critical shear stress, and the associated critical shear velocity related to d_{84} as per Brownlie (1981). Then, we estimated the critical velocity $U_{c,d_{84}}$ employing the logarithmic law of the wall, as per Melville (1997). To assess how the critical armoring condition is affected by the exact definition of $U_{c,d_{84}}$, we conducted a dedicated sensitivity analysis, using other approaches available from the literature to estimate it (see Appendix SI and Fig. S1 in Supplemental Material for more details). The results from this analysis indicate a maximum variation of approximately 10% in $U_{c,d_{84}}$ across the approaches tested.

In light of the data-stratification observed at low U/U_c in Fig. 3a, we defined a new live-bed scour function $S_{e,LB}$ based on $S_e{}'$ and including the sediment gradation function $f_3(\sigma_g)$ as modeled in clear-water (Eq. 11), i.e.

$$S_{e,LB} = \frac{\frac{y_{se}g}{U^2} f_2\left(\frac{a}{d}\right)}{\frac{\rho}{\rho_s-\rho}\left(C_d\right)^{2/3}\left(\frac{a}{d}\right)^{2/3} f_3(\sigma_g)} = \Phi'\left(\frac{U}{U_{c,d_{84}}}\right). \tag{12}$$

When $S_{e,LB}$ is plotted against $U/U_{c,d_{84}}$ (Fig. 3b), data for non-uniform sediments show a clear transition in regimes at $U/U_{c,d_{84}} \approx 0.8$, which can be identified as the critical armoring condition. Below this threshold, experimental data consistently align around $S_{e,LB} \approx 1$, supporting the assumption that sediment gradation affects scour depth as in clear-water conditions when the critical armoring condition is not reached. Therefore, for $U/U_{c,d_{84}} < 0.8$, $S_{e,LB}$ appears suitable for estimating the scour depth. Conversely, above the critical armoring condition the scour depth is independent of σ_g and appears to depend only on the flow intensity (Fig. 3a) as for uniform sediments.

In Fig. 3c the corrected live-bed scour function $S_e{}'$ (Eq. 9) is recalculated for both uniform and non-uniform sediments datasets, focusing on experiments characterized by $U/U_{c,d_{84}} \geq 0.8$. Given the excellent alignment displayed, we deduce that the function $\Phi(U/U_c)$ (Eq. 8) estimated for uniform sediments is appropriate to model the impact of flow intensity on scour depth in

fully developed live-bed conditions independently of the sediment mixture (solid line in Fig. 3c), confirming that in such conditions the effect of armoring becomes almost irrelevant. A slight residual dependence of data on σ_g is present for $U/U_c < 3$. This residual armoring effect could be easily modeled, however it appears to be weak and can be safely neglected, resulting in a conservative approach due to the scour-reducing effect of armoring.

DISCUSSION

Based on the results of our analysis, we can establish a final formulation for y_{se}, which varies depending on the flow conditions and sediment transport regime. In clear-water conditions ($U/U_c \leq 1$), y_{se} is determined from Eq. 10 as

$$y_{se} = \frac{\frac{\rho}{\rho_s-\rho}\frac{U^2}{g}(C_d)^{2/3}\left(\frac{a}{d}\right)^{2/3} f_3(\sigma_g)}{f_1\left(\frac{d}{\eta}\right) f_2\left(\frac{a}{d}\right)}, \tag{13}$$

whereas in live-bed conditions ($U/U_c > 1$), y_{se} is determined by one of the following equations:

$$y_{se} = \frac{\frac{\rho}{\rho_s-\rho}\frac{U^2}{g}(C_d)^{2/3}\left(\frac{a}{d}\right)^{2/3} f_3(\sigma_g)}{f_2\left(\frac{a}{d}\right)}, \tag{14a}$$

$$y_{se} = \frac{\frac{\rho}{\rho_s-\rho}\frac{U^2}{g}(C_d)^{2/3}\left(\frac{a}{d}\right)^{2/3} \Phi\left(\frac{U}{U_c}\right)}{f_2\left(\frac{a}{d}\right)}. \tag{14b}$$

Eq. 14a (derived from Eq. 12) applies when armoring occurs, that is, below the critical armoring condition ($U/U_{c,d_{84}} < 0.8$) with high sediment gradation ($\sigma_g \geq 2$), whereas Eq. 14b (derived from Eq. 9) applies when the effects of armoring are negligible (i.e. $\sigma_g < 2$ and/or $U/U_{c,d_{84}} \geq 0.8$). The various functions $f_1(d/\eta)$, $f_2(a/d)$, $\Phi(U/U_c)$ and $f_3(\sigma_g)$ employed in Eqs. 13-14 are reported in Eq. 5, Eq. 6, Eq. 8 and Eq. 11, respectively. Application examples of the formula can be found in Appendix SII.

Overall performance of the proposed formula

In this section, we assess the reliability of the proposed formula through a systematic comparison of its performance with that of the most employed approaches proposed in the literature. Towards

this end we employ several metrics that quantify the predictive accuracy of y_{se}. This validation procedure is initially conducted using laboratory data and then extended to some of the available field data from the literature.

The reference formulas selected for comparison are those proposed by Sheppard et al. (2014) (S/M), Richardson and Davis (2001) (HEC-18), Sheppard and Miller (2006) (SM06), Froelich (1988) (F88), and Melville (1997) (M97). Sheppard et al. (2014) demonstrated that S/M is the most accurate model among the 23 evaluated. HEC-18, SM06, and M97 are recognized by Ettema et al. (2011) as leading methods for pier scour estimation. F88 is considered one of the most reliable formulations derived from field measurements (Sheppard et al. 2011). Detailed descriptions of all models are provided in the Supplemental Material (Appendix SIII). It is worth noting that S/M, SM06 and F88 do not incorporate correction factors to account for sediment non-uniformity, presumably in view of adopting a conservative approach that neglects the reduction of local scour caused by armoring-effects. We based our comparative analysis between the measured scour $y_{se,m}$ and the predicted scour depth $y_{se,p}$ on four complementary performance metrics:

1. the mean relative error $\overline{E_m} = \frac{1}{N} \sum \frac{|y_{se,p} - y_{se,m}|}{y_{se,m}} \times 100$, where N is the number of data points, as employed by MB15 and CGM20;
2. the sum of squared relative errors $SSE = \frac{\sum (y_{se,p} - y_{se,m})^2}{\sum (y_{se,m})^2} \times 100$, following Sheppard et al. (2014);
3. the Nash–Sutcliffe efficiency coefficient $NS = 1 - \frac{\sum (y_{se,m} - y_{se,p})^2}{\sum (y_{se,m} - \overline{y_{se,m}})^2}$, as adopted by Franzetti et al. (2022), which evaluates the accuracy of a predictive model in reproducing experimental data ($NS = 1$ indicates perfect agreement, whereas $NS < 0$ indicates that the model perform worse than simply using the mean of the experimental measurements) ; and
4. the percentage of predictions, P_{out}, falling outside a 30% error margin, inspired by the approach of Franzetti et al. (2022).

The dataset of laboratory experiments involved in the analysis encompasses a total of 622 measurements, approximately balanced between clear-water and live-bed conditions, with over 200

experiments involving non-uniform sediments up to $\sigma_g = 5.5$ (see Table 1). A thorough literature review was carried out to include a large number of published data neglecting only those that were not consistent with the assumptions underlying our model, such as clear-water data collected far from equilibrium conditions (i.e. in short-duration experiments), or live-bed data not filtered from the effects induced by the passage of bedforms.

Fig. 4 shows a comparison between the measured scour depth $y_{se,m}$ in laboratory experiments and the predicted scour depth $y_{se,p}$ estimated according to our formula (panel a), S/M (panel b), HEC-18 (panel c), SM06 (panel d), F88 (panel e) and M97 (panel e). Table 2 reports the values of the performance metrics, evaluated over specific subsets, the full laboratory dataset and the selected field data. At a first glance, it is evident that our formula leads to an improved data collapse with respect to the others. The improved performance remains consistent across both uniform and non-uniform sediment conditions, as well as across clear-water and live-bed regimes. In general, the other formulas exhibit a lower performance across all the metrics. Exceptions are noted for S/M, SM06 and M97 in clear-water conditions with uniform sediments which have a few comparable or slightly better indicators. As previously discussed, S/M, SM06 and F88 are specifically designed for uniform sediments. Accordingly, their accuracy diminishes when applied to non-uniform sediments data, particularly in clear-water conditions. S/M exhibits a performance very similar to SM06, since it retains the same underlying structure while introducing minor adjustments that reduce underprediction and make it more robust as a design tool. F88 shows a good accuracy in predicting scour depth in live-bed conditions with uniform sediments, reflecting the fact that it was derived from field data under such conditions. HEC-18 also demonstrates greater accuracy for uniform than for non-uniform sediments. This discrepancy arises from the limited applicability of the corrective function used, designed to account for armoring effects only for very coarse sediments. Given that few data respect this criterion, the HEC-18 formula exhibits significantly reduced performance when applied to non-uniform sediments. M97 accounts for the occurrence of armoring by introducing a characteristic armoring velocity that marks the transition between clear-water and live-bed conditions in the presence of non-uniform sediments. However,

even this model exhibits limited accuracy when applied to non-uniform sediments particularly in clear-water conditions.

Another key factor contributing to the lower performance of the reference formulas is their inherently conservative nature. Being primarily intended for design purposes, these models intentionally tend to overestimate scour depths and prioritize accuracy at large values of $y_{se,m}$ (i.e. $y_{se,m} > 0.2$ m), which are more relevant to practical applications. Our formula, instead, appears more suitable for the assessment rather than the design phase, as it intends to predict, rather than over-predict, scour depths. Therefore, to extend the applicability of the model to the design phase, we would recommend the introduction of a safety factor. Specifically, following the approach of (Froelich 1988), we observe that the normalized measured scour depth $y_{se,m}/a$ is consistently lower than the normalized predicted scour depth $y_{se,p}/a$ (given by Eqs. 13-14) plus 1. Consequently, adding the value of the pier diameter a to the predicted scour depth systematically overestimates the entire laboratory dataset, thereby providing an appropriate safety factor.

We now extend the application of our formula to a series of scour measurements collected in the field. It is important to note that field data typically exhibit greater uncertainty due to factors such as the unknown maturity of the scour hole and the inherent challenges in data collection. However, field measurements offer the significant advantage of eliminating scale effects (Sheppard et al. 2014). Data were extracted from the appendix of Sheppard et al. (2011) and subsequently filtered to retain only those compatible with the application of our model. Specifically, we excluded all data points identified as outliers by Sheppard et al. (2014), as well as those with missing or ambiguous key parameters. Regarding this latter filter, when multiple cases shared identical geometric, hydraulic, and granulometric variables, but reported different scour depths, we retained only the measurement corresponding to the highest recorded scour depth. Additionally, cases involving complex pier shapes (i.e. shapes other than circular or square) were omitted. This filtering step is required because the available information for non-standard geometries are insufficient to determine a reliable drag coefficient C_d. Moreover, it is important to note that, in our theoretical framework, C_d refers specifically to the portion of the pier exposed to scour, which, in most cases, corresponds

to the foundation elements for which, however, details of the geometry are also not reported in the literature. This makes it difficult to choose an appropriate value of C_d. As a first approximation, we employed the C_d of the pier above the foundation elements assuming it to be prismatic in and out of the sediment bed as encountered in most laboratory data sets. This filtering process resulted in a final dataset of 68 measurements (see the field data subset in Table 1), all characterized by non-uniform sediments, as expected in field conditions. We computed the critical velocity U_c as described in the previous sections of the paper, and we modified the drag coefficient for squared piers as function of their aspect ratio, following Çengel and Cimbala (2013).

Fig. 5 presents the comparison between our model and the previously introduced literature formulas in predicting scour depth for the field dataset, using the same panel arrangement as in Fig. 4. Performance metrics for these field data are summarized in Table 2. Despite the approximations used for estimating C_d, the results appear to be very promising, as the newly proposed formula outperforms all the others across all considered metrics. As per laboratory data, the alternative formulas tend to significantly overestimate the local scour depth. In contrast, our formula provides less biased estimates. Clearly, with respect to laboratory data, uncertainties of predictions are significantly higher and, given the complexity of field conditions as well as challenges in data collection, it is hard to explain why with confidence. Nevertheless, in what follows, the limitations of the proposed formula are identified and discussed with a view to assess its applicability in engineering practice and to identify avenues for future research.

Applicability and limitations of the formula

As shown by the comparison with the best formulas available in literature, our approach effectively predicts local scour depths when applied to laboratory and, with appropriate caution, field data. Its predictive capability appears to be fairly independent of sediment properties (provided that the sediments are cohesionless) and of flow regime, with the exception of a slight decrease in performance in clear-water conditions with non-uniform sediments (see Fig. 4) and, as reported by CGM20, with coarse sediments, whereby bed permeability effects are not accounted for in the definition of both τ and τ_c. We recommend that future research efforts should be dedicated

to clarify the role of bed permeability and sediment non-uniformity in dictating shear stress and critical shear stress in local scour holes.

The proposed formula has been developed and tested only for isolated prismatic piers with a simple geometry. In principle, complex-geometry effects may be incorporated into $C_d^{2/3}$ (see MB15), which serves as the equivalent of the so-called shape-parameters commonly employed in the literature. Indeed, a comparison between the corrective effects of our $C_d^{2/3}$ and those reported by Ettema et al. (2011) for their shape coefficients, reveals only minor differences (see Fig. S2 and Table S1 in Appendix SIV), suggesting that $C_d^{2/3}$ or existing shape factors could be used interchangeably. This is a promising result but further studies are required to identify appropriate methods for estimating drag coefficients associated with complex pier-foundation geometries and relate them to effects on local scour depths.

Some characteristic features of the proposed approach and associated limitations can be obtained by discussing the relation between the normalized scour depth y_{se}/a and the flow intensity U/U_c. The experimental data reported in Fig. 6a indicate that, in presence of negligible sediment gradation effects (i.e. $\sigma_g < 2$), the shift from clear-water to live-bed conditions is abrupt, with y_{se}/a reaching a clear-water peak and then sharply decreasing as U/U_c exceeds 1 (Melville and Chiew 1999). As the degree of sediment non-uniformity increases, the occurrence of armoring delays the onset of live-bed conditions to higher flow intensities and reduces the peak scour depth, resulting in a smoother transition (Melville 2008). In Fig. 6b we plot the trend of y_{se}/a predicted with our formula as function of U/U_c for increasing values of σ_g. These curves were obtained by applying Eqs. 13-14 to hypothetical laboratory experiments performed in a flume with adjustable slope such that the water depth can be kept constant as the bulk flow velocity increases, hence U_c can be kept constant while U/U_c increase progressively (see the caption of Fig. 6 for details).

A visual comparison of Figs. 6a and 6b clearly shows that our formula effectively replicates the observed trends. As the data exhibit an evident jump in the transition between clear-water and live-bed conditions (i.e., at $U/U_c \approx 1$), the formula introduces a discontinuity to reflect this behavior. It should be noted that such a discontinuity, particularly evident for uniform sediments,

is probably unphysical and may well be an experimental artifact, partly due to the long-standing difficulties in defining an effective critical condition of incipient sediment motion, here quantified with U_c (see e.g. Pähtz et al. 2020). In reality, the onset of live-bed conditions and its effects on scour are probably diffused in a sizable transition band (e.g. $0.9 < U/U_c < 1.5$), rather than immediately after the flow intensity exceeds 1. However, this is hard to observe from experimental data (Fig. 6a) and consequently to model (Fig. 6b). Classical approaches tend to avoid this issue by neglecting the discontinuity present in the data and systematically overestimating scour depth within the transition region (see, e.g., Melville 1997; Sheppard et al. 2014). A less conservative and more realistic approach, would be to modulate Φ (Eq. 8) with e.g. a decay function forcing a smooth transition to $S_e' = 1$ within a narrow range of U/U_c approaching unity. However, we believe that the potential improvement in predictive accuracy would not justify the increased complexity associated with the introduction of ad-hoc transition functions, also given that most engineering applications involve well-developed live-bed conditions. Nevertheless, for particular applications falling within this narrow transitional range, we recommend estimating y_{se} by applying both the clear-water and live-bed formulations, and adopting the larger of the two estimates in order to reduce the risk of underestimations.

For $\sigma_g \geq 2$, Eq. 14 accounts for the effect of armoring by introducing two more discontinuities in the behavior of y_{se}/a versus U/U_c. The first discontinuity is associated with the onset of live-bed conditions and the initiation of sediment motion ($U/U_c = 1$), as discussed above. The second discontinuity coincides with the critical armoring condition ($U/U_{c,d_{84}} = 0.8$). For $U/U_{c,d_{84}} < 0.8$, the armored layer cannot be eroded, resulting in scour estimates consistent with those for clear-water conditions. Within this range, we validated Eq. 14a with the very few available experimental data (see Fig. 3b). While the model performs reasonably well, due to the small size of the dataset employed, it may present some limitations when applied to different datasets. Above the critical armoring condition (i.e. for $U/U_{c,d_{84}} \geq 0.8$), the high sediment transport rates mask any armoring effect and the scour depth is modeled as if sediments were uniform (Eq. 14b).

Clearly, as per the transition between clear-water and live-bed conditions, also these two dis-

continuities result from the definition of sharp boundaries between different behaviors, which serve well modeling purposes but do not necessarily align with the physics of sediment transport. Also in these cases, when engineering applications require estimating local scour around these discontinuities, it is important to proceed with caution and adopt the most conservative estimate derived from the surrounding values.

SUMMARY AND CONCLUSION

This study builds upon the works of Manes and Brocchini (2015) and Coscarella et al. (2020) and introduces a novel formula (or set of formulas) for predicting the equilibrium scour depth at bridge piers. With respect to previous works, the proposed approach accounts for effects of low relative coarseness in live-bed conditions and sediment non-uniformity. Regarding the effects of low relative coarseness, we demonstrated that the dedicated corrective function introduced by Coscarella et al. (2020) for clear-water conditions can be reliably applied to live-bed conditions too. The influence of non-uniform sediments and, consequently, the occurrence of armoring, is modeled via a sediment gradation function $f_3(\sigma_g)$ and introducing the critical armoring threshold concept for live-bed conditions.

The proposed formula demonstrates improved accuracy over existing leading methods in reproducing a large amount of experimental data from laboratory studies. It also shows enhanced performance when applied to selected field datasets, particularly where sufficient information on pier geometry allows for confident application. Unlike traditional approaches, which tend to provide conservative scour depth estimates, this formula is tailored for risk assessment rather than design scenarios. However, when including an appropriate safety margin, it can be adapted for design applications as well. For example, adding the value of the pier diameter a to the predicted scour depth allows for conservatively overestimating all laboratory data and more than 95% of the field data.

At a fundamental level, future refinements to the proposed approach should focus on: (i) clarifying the influence of permeability on turbulent momentum transport and the initiation of sediment motion within scour holes in coarse sediment beds; (ii) improving current methods to

incorporate sediment non-uniformity effects and expanding experimental datasets to cover a broader range of grain size distributions (higher values of σ_g); and (iii) developing reliable techniques for estimating the drag coefficient (C_d) to capture the effects of complex pier and foundation geometries.

DATA AVAILABILITY STATEMENT

All data, models, and code generated or used during the study appear in the submitted article.

ACKNOWLEDGMENTS

Financial support was provided by the project RETURN (multi-Risk sciEnce for resilienT commUnities undeR a changiNg climate) funded by the Italian Ministry of University and Research with funds from the Next Generation EU with grant agreement no. 1551 – 10/11/2022. The authors thanks Silvio Franzetti, Francesco Ballio, Alessio Radice and Daniel Rebai for their helpful comments provided during the development of this work.

SUPPLEMENTAL MATERIALS

Appendixes SI (with Fig. S1), SII, SIII and SIV (with Fig. S2 and Table S1) are reported in a unique supplemental material document, available online in the ASCE Library (`ascelibrary.org`).

REFERENCES

Brownlie, W. R. (1981). "Prediction of flow depth and sediment discharge in open channels." *Report no. 124, school of engineering*, California Institute of Technology, Pasadena, CA.

Çengel, Y. A. and Cimbala, J. M. (2013). *Fluid mechanics: fundamentals and applications*. McGraw Hill.

Chee, R. K. W. (1982). "Live-bed scour at bridge sites." M.S. thesis, University of Auckland, Auckland, New Zealand.

Chiew, Y. M. (1984). "Local scour at bridge piers." Ph.D. thesis, Dept. of Civil Engineering, University of Auckland, Auckland, New Zealand.

Chiew, Y. M. (1991). "Bed features in nonuniform sediments." *J. Hydraul. Eng.*, ASCE, 117(1), 116–120 10.1061/(ASCE)0733-9429(1991)117:1(116).

561 Coscarella, F., Gaudio, R., and Manes, C. (2020). "Near-bed eddy scales and clear-water local
562 scouring around vertical cylinders." *J. Hydraul. Res.*, Taylor and Francis Ltd., 58(6), 968–981
563 10.1080/00221686.2019.1698668.
564 Dey, S. (2014). *Fluvial hydrodynamics*. Springer Berlin, Heidelberg, 1 edition.
565 Dey, S., Bose, S. K., and Sastry, G. L. N. (1995). "Clear water scour at circular piers: a model." *J.*
566 *Hydraul. Eng.*, ASCE, 121(12), 869–876 10.1061/(ASCE)0733-9429(1995)121:12(869).
567 Ettema, R. (1976). "Influence of bed material gradation on local scour." *Report no. 124, school of*
568 *engineering*, University of Auckland.
569 Ettema, R. (1980). "Scour at bridge piers." *Report no. 216, school of engineering*, University of
570 Auckland.
571 Ettema, R., Constantinescu, G., and Melville, B. W. (2011). "Evaluation of bridge scour research:
572 Pier scour processes and predictions." *Nchrp web-only rep. 175*, National Cooperative Highway
573 Program, Washington, DC.
574 Ettema, R., Kirkil, G., and Muste, M. (2006). "Similitude of large-scale turbulence in experiments
575 on local scour at cylinders." *J. Hydraul. Eng.*, ASCE, 132(1), 33–40 10.1061/(ASCE)0733-
576 9429(2006)132:1(33).
577 Ettema, R., Melville, B. W., and Barkdoll, B. (1998). "Scale effect in pier-scour experiments." *J.*
578 *Hydraul. Eng.*, ASCE, 124(6), 639–642 10.1061/(ASCE)0733-9429(1998)124:6(639).
579 Franzetti, S., Radice, A., Rebai, D., and Ballio, F. (2022). "Clear water scour at circular piers:
580 A new formula fitting laboratory data with less than 25% deviation." *J. Hydraul. Eng.*, ASCE,
581 148(10), 04022021 10.1061/(ASCE)HY.1943-7900.0002009.
582 Froelich, D. C. (1988). "Analysis of onsite measurements of scour at piers." *Proc., 1988 National*
583 *Conf. on Hydraulic Engineering*, ASCE, 534–539.
584 Gioia, G. and Bombardelli, F. A. (2001). "Scaling and similarity in rough channel flows." *Phys.*
585 *Rev. Lett.*, APS, 88(1), 014501 10.1103/PhysRevLett.88.014501.
586 Guo, J., Suaznabar, O., Shan, H., and Shen, J. (2012). "Pier scour in clear-water conditions with
587 non-uniform bed materials." *Fhwa-hrt-12-022*, U.S. Federal Highway Administration, Office of

588 Infrastructure, Research and Development, McLean, VA.

589 Lança, R. M., Fael, C. S., Maia, R. J., Pêgo, J. P., and Cardoso, A. H. (2013). "Clear-water
590 scour at comparatively large cylindrical piers." *J. Hydraul. Eng.*, ASCE, 139(11), 1117–1125
591 10.1061/(ASCE)HY.1943-7900.0000788.

592 Lee, S. O. and Sturm, T. W. (2009). "Effect of sediment size scaling on physical modeling
593 of bridge pier scour." *J. Hydraul. Eng.*, ASCE, 135(10), 793–802 10.1061/(ASCE)HY.1943-
594 7900.0000091.

595 Maddison, B. (2012). "Scour failure of bridges." *Proc. Inst. Civ. Eng. ForensicEng.*, Thomas Telford
596 Ltd, 165(1), 39–52 10.1680/feng.2012.165.1.39.

597 Manes, C. and Brocchini, M. (2015). "Local scour around structures and the phenomenology of
598 turbulence." *J. Fluid Mech.*, Cambridge University Press, 779, 309–324 10.1017/jfm.2015.389.

599 Manes, C., Pokrajac, D., Nikora, V., Ridolfi, L., and Poggi, D. (2011). "Turbulent friction in flows
600 over permeable walls." *Geoph. Res. Lett.*, AGU, 38(3) 10.1029/2010GL045695.

601 Manes, C., Ridolfi, L., and Katul, G. (2012). "A phenomenological model to describe turbulent
602 friction in permeable-wall flows." *Geoph. Res. Lett.*, AGU, 39(14) 10.1029/2012GL052369.

603 Melville, B. W. (1984). "Live-bed scour at bridge piers." *J. Hydraul. Eng.*, ASCE, 110(9), 1234–
604 1247 10.1061/(ASCE)0733-9429(1984)110:9(1234).

605 Melville, B. W. (1997). "Pier and abutment scour: integrated approach." *J. Hydraul. Eng.*, ASCE,
606 123(2), 125–136 10.1061/(ASCE)0733-9429(1997)123:2(125).

607 Melville, B. W. (2008). "The physics of local scour at bridge piers." *Proc., 4th Int. Conf. on Scour
608 and Erosion*, ISSMGE, 28–40.

609 Melville, B. W. and Chiew, Y. M. (1999). "Time scale for local scour at bridge piers." *J. Hydraul.
610 Eng.*, ASCE, 125(1), 59–65 10.1061/(ASCE)0733-9429(1999)125:1(59).

611 Melville, B. W. and Coleman, S. E. (2000). *Bridge Scour*. Water Resources Publications, LLC.

612 Melville, B. W. and Sutherland, A. J. (1988). "Design method for local scour at bridge piers." *J.
613 Hydraul. Eng.*, ASCE, 114(10), 1210–1226 10.1061/(ASCE)0733-9429(1988)114:10(1210).

614 Meyer-Peter, E. and Müller, R. (1948). "Formulas for bed-load transport.

Molinas, A. (2004). "Bridge scour in nonuniform sediment mixtures and in cohesive materials: Synthesis report." *Fhwa-rd-03-083*, U.S. Federal Highway Administration, Office of Infrastructure, Research and Development, McLean, VA.

Mueller, D. S. and Wagner, C. R. (2005). "Field observations and evaluations of streambed scour at bridges." *Fhwa-rd-03-052*, U.S. Federal Highway Administration, Office of Infrastructure, Research and Development, McLean, VA.

Pähtz, T., Clark, A. H., Valyrakis, M., and Durán, O. (2020). "The physics of sediment transport initiation, cessation, and entrainment across aeolian and fluvial environments." *Rev. Geophys.*, AGU, 58(1), e2019RG000679 10.1029/2019RG000679.

Pandey, M., Sharma, P. K., Ahmad, Z., and Karna, N. (2018). "Maximum scour depth around bridge pier in gravel bed streams." *Nat. Hazard.*, Springer, 91, 819–836 10.1007/s11069-017-3157-z.

Parker, G., Klingeman, P. C., and McLean, D. G. (1982). "Bedload and size distribution in paved gravel-bed streams." *J. Hydr. Div*, ASCE, 108(4), 544–571 10.1061/JYCEAJ.0005854.

Raikar, R. V. and Dey, S. (2005). "Clear-water scour at bridge piers in fine and medium gravel beds." *Can. J. Civ. Eng.*, NRC Research Press Ottawa, Canada, 32(4), 775–781 10.1139/l05-022.

Raudkivi, A. J. (1986). "Functional trends of scour at bridge piers." *J. Hydraul. Eng.*, ASCE, 112(1), 1–13 10.1061/(ASCE)0733-9429(1986)112:1(1).

Raudkivi, A. J. and Ettema, R. (1983). "Clear-water scour at cylindrical piers." *J. Hydraul. Eng.*, ASCE, 109(3), 338–350 10.1061/(ASCE)0733-9429(1983)109:3(338).

Richardson, E. V. and Davis, S. R. (2001). "Evaluating scour at bridges—fourth edition." *Hydraulic engineering circular 18 (hec-18)*, U.S. Federal Highway Administration, Washington, DC.

Shen, H. W., Schneider, V. R., and Karaki, S. (1969). "Local scour around bridge piers." *J. Hydr. Div*, ASCE, 95(6), 1919–1940 10.1061/JYCEAJ.0002197.

Sheppard, D. M., Melville, B., and Demir, H. (2014). "Evaluation of existing equations for local scour at bridge piers." *J. Hydraul. Eng.*, ASCE, 140(1), 14–23 10.1061/(ASCE)HY.1943-7900.0000800.

Sheppard, D. M. and Miller, W. (2006). "Live-bed local pier scour experiments." *J. Hydraul. Eng.*,

642 ASCE, 132(7), 635–642 10.1061/(ASCE)0733-9429(2006)132:7(635).
643 Sheppard, D. M., Odeh, M., and Glasser, T. (2004). “Large scale clear-water local pier
644 scour experiments.” *J. Hydraul. Eng.*, ASCE, 130(10), 957–963 10.1061/(ASCE)0733-
645 9429(2004)130:10(957).
646 Sheppard, M., Demir, H., and Melville, B. W. (2011). “Scour at wide piers and long skewed piers.”
647 *Nchrp rep. 682*, National Cooperative Highway Program, Washington, DC.
648 Shields, A. (1936). “Anwendung der aehnlichkeitsmechanik und der turbulenzforschung auf die
649 geschiebebewegung.” Ph.D. thesis, Technical University Berlin,
650 Wardhana, K. and Hadipriono, F. C. (2003). “Analysis of recent bridge failures in the united states.”
651 *J. Perform. Constr. Facil.*, ASCE, 17(3), 144–150 10.1061/(ASCE)0887-3828(2003)17:3(144).

List of Tables

TABLE 1. Range of the main experimental variables for the datasets analyzed in the present work.

Source	a (m)	U (m s^{-1})	U_c (m s^{-1})	h (m)	d_{50} (mm)	σ_g	$y_{se,m}$ (m)
Clear-water, uniform sediments							
Ettema (1980)	0.03-0.24	0.20-1.21	0.24-1.27	0.02-0.60	0.24-7.80	1.10	0.02-0.35
Dey et al. (1995)	0.06-0.08	0.17-0.26	0.22-0.27	0.04-0.05	0.26-0.58	1.30	0.05-0.10
Melville (1997)	0.02-0.77	0.21-0.33	0.31-0.39	0.05-0.20	0.80-0.90	1.40	0.02-0.44
Melville and Chiew (1999)	0.04-0.08	0.18-0.32	0.33-0.41	0.05-0.20	0.96	1.40	0.03-0.14
Sheppard et al. (2004)	0.11-0.91	0.39-0.76	0.45-1.02	0.17-1.90	0.80-2.90	1.40	0.23-1.39
Ettema et al. (2006)	0.06-0.41	0.46	0.54	1.00	1.05	1.10	0.11-0.44
Pandey et al. (2018)	0.07-0.12	0.28-1.01	0.32-1.24	0.08-0.20	0.40-11.3	1.20	0.02-0.16
Live-bed, uniform sediments							
Shen et al. (1969)	0.15	0.29-1.02	0.26-0.29	0.11-0.27	0.24	1.40	0.13-0.21
Chee (1982)	0.05-0.10	0.30-1.20	0.26-0.47	0.10	0.24-1.40	1.20-1.30	0.05-0.14
Chiew (1984)	0.03-0.05	0.31-1.84	0.27-0.73	0.17-0.34	0.24-3.20	1.18-1.33	0.03-0.10
Sheppard and Miller (2006)	0.15	0.55-2.16	0.25-0.41	0.20-0.43	0.27-0.84	1.30	0.17-0.30
Clear-water, non-uniform sediments							
Ettema (1976)	0.10	0.35-0.96	0.37-1.01	0.60	0.55-4.1	1.60-4.60	0.04-0.22
Molinas (2004)	0.02-0.22	0.20-0.50	0.45-0.57	0.19-0.40	0.55-0.75	2.24-3.40	0.01-0.21
Sheppard et al. (2004)	0.11-0.92	0.29-0.31	0.34-0.35	1.19-1.81	0.22	1.50	0.17-0.97
Raikar and Dey (2005)	0.08	0.76-1.10	0.79-1.16	0.25	4.10-14.30	1.51-2.93	0.03-0.19
Guo et al. (2012)	0.03-0.14	0.28-0.38	0.36-0.45	0.20	0.46-0.89	2.10-2.50	0.02-0.13
Live-bed, non-uniform sediments							
Shen et al. (1969)	0.15-0.92	0.38-0.66	0.30-0.35	0.18-0.67	0.46	2.20	0.17-0.67
Chiew (1984)	0.03-0.07	0.35-1.92	0.34-0.45	0.17	0.60-1.45	2.00-5.50	0.01-0.12
Field data							
Mueller and Wagner (2005)	0.30-5.49	0.21-2.41	0.35-1.75	0.21-22.50	0.40-7.50	1.60-9.00	0.31-7.19
Froelich (1988)	2.41	0.95	0.54	3.44	0.80	2.30	2.78

TABLE 2. Performance comparison for different subsets of the dataset

	Our formula	S/M	HEC-18	SM06	F88	M97
Clear-water, uniform sediments						
$\overline{E_m}$ (%)	22.7	34.5	77.0	28.7	48.9	36.0
SSE (%)	4.3	3.2	8.0	3.3	9.4	14.0
NS	0.9	0.9	0.9	0.9	0.9	0.8
P_{out} (%)	27.1	40.9	45.2	35.1	34.0	26.1
Live-bed, uniform sediments						
$\overline{E_m}$ (%)	11.3	32.1	79.1	32.1	16.2	52.4
SSE (%)	2.9	7.9	39.7	7.9	4.0	35.9
NS (%)	0.9	0.7	<0	0.7	0.9	<0
P_{out} (%)	2.4	49.2	91.8	49.2	15.0	84.1
Clear-water, non-uniform sediments						
$\overline{E_m}$ (%)	24.6	214.8	186.5	194.8	202.3	165.2
SSE (%)	8.6	103.9	67.9	95.5	88.1	109.2
NS	0.8	<0	<0	<0	<0	<0
P_{out} (%)	31.9	92.4	88.2	90.8	88.2	94.1
Live-bed, non-uniform sediments						
$\overline{E_m}$ (%)	21.2	75.0	137.8	77.7	43.6	69.6
SSE (%)	2.1	31.6	49.8	29.1	72.0	153.5
NS	1.0	0.4	0.1	0.5	<0	<0
P_{out} (%)	30.6	61.1	93.5	67.6	46.3	87.0
Full dataset						
$\overline{E_m}$ (%)	19.0	75.2	109.2	70.1	66.4	72.0
SSE (%)	4.5	18.0	22.3	16.9	22.2	37.3
NS	0.9	0.7	0.6	0.7	0.6	0.4
P_{out} (%)	20.4	57.0	77.3	56.1	40.2	69.0
Field data						
$\overline{E_m}$ (%)	92.7	236.1	135.4	232.8	315.4	327.4
SSE (%)	28.5	80.0	77.5	77.5	339.8	417.8
NS	0.4	<0	<0	<0	<0	<0
P_{out} (%)	54.4	76.5	67.6	72.0	83.8	92.6

List of Figures

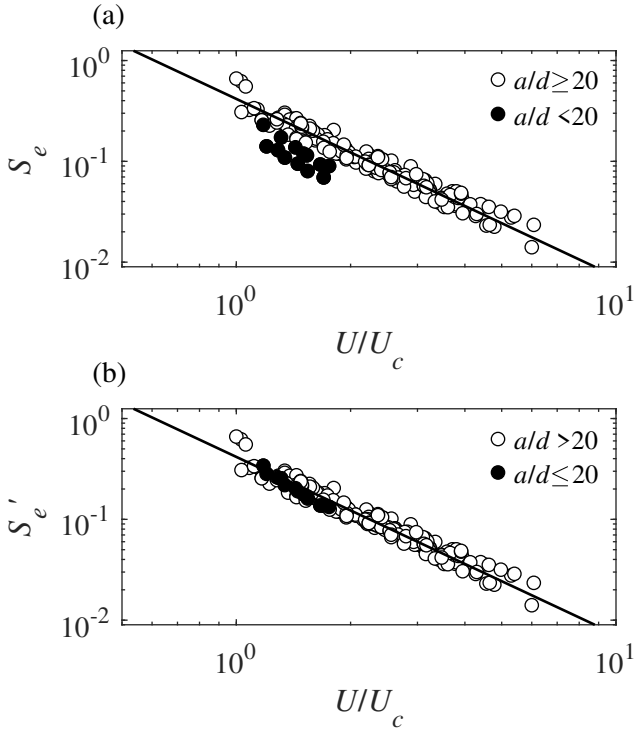

Fig. 1. (a) Live-bed scour function for uniform sediments S_e [Eq. (3)] and (b) corrected live-bed scour function for uniform sediments S_e', versus flow intensity U/U_c [Eq. (9)]. All the data points appearing in this figure pertain to experiments carried out in live-bed conditions with uniform sediments (Table 1). The solid line represents the flow intensity function $\Phi(U/U_c)$ [Eq. 8].

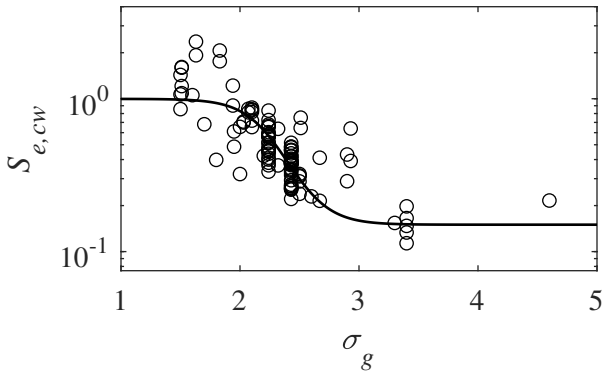

Fig. 2. Clear-water scour function for non-uniform sediments $S_{e,CW}$ versus sediment gradation σ_g [Eq. 10]. All data refer to experiments carried out in clear-water conditions with nonuniform sediments (Table 1). The solid line represents the sediment gradation function $f_3(\sigma_g)$ [Eq. 11].

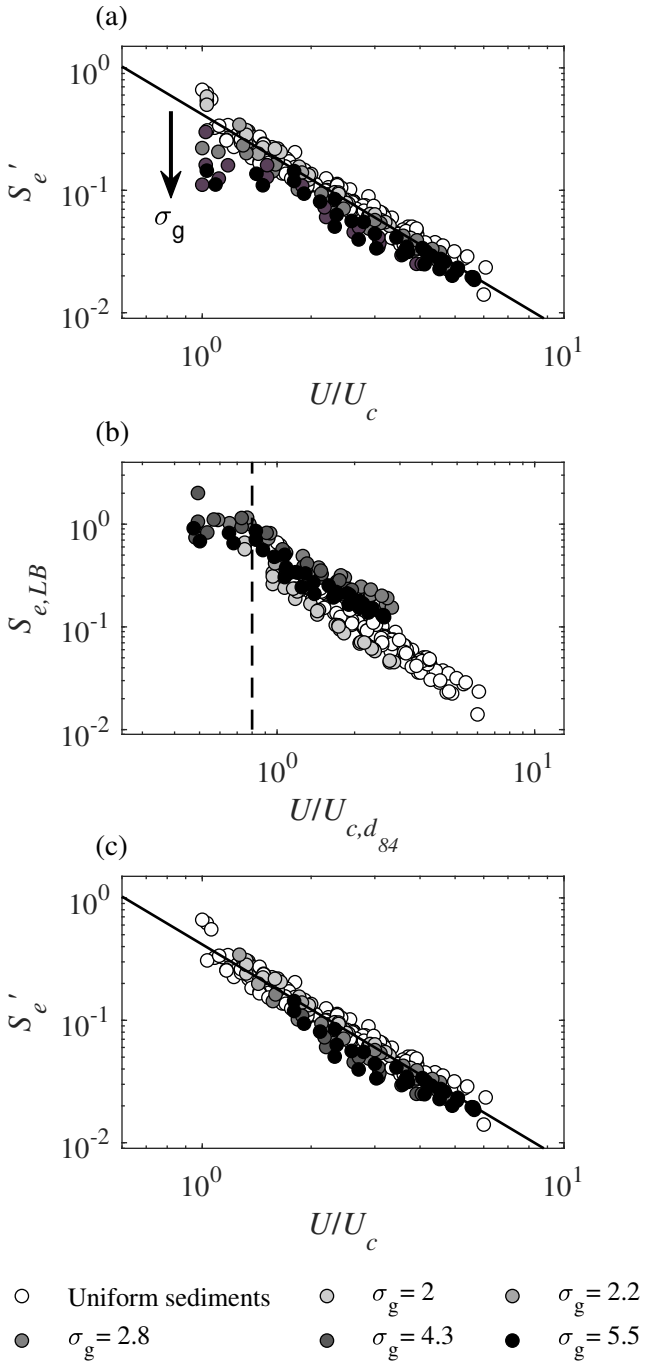

Fig. 3. (a) Corrected live-bed scour function for uniform sediments S_e' versus flow intensity U/U_c [Eq. (9)]; (b) live-bed scour function for nonuniform sediments $S_{e,LB}$ versus $U/U_{c,d_{84}}$ [Eq. (12)]; and (c) corrected live-bed scour function for uniform sediments S_e' calculated for data with $U/U_{c,d_{84}} \geq 0.8$ versus flow intensity U/U_c [Eq. (9)]. Data collected in live-bed conditions with both uniform and nonuniform sediments are used (Table 1). The dashed line in (b) represents the critical armor condition $U/U_{c,d_{84}} = 0.8$, while the solid line in (a) and (c) the flow intensity function $\Phi(U/U_c)$ [Eq. 8].

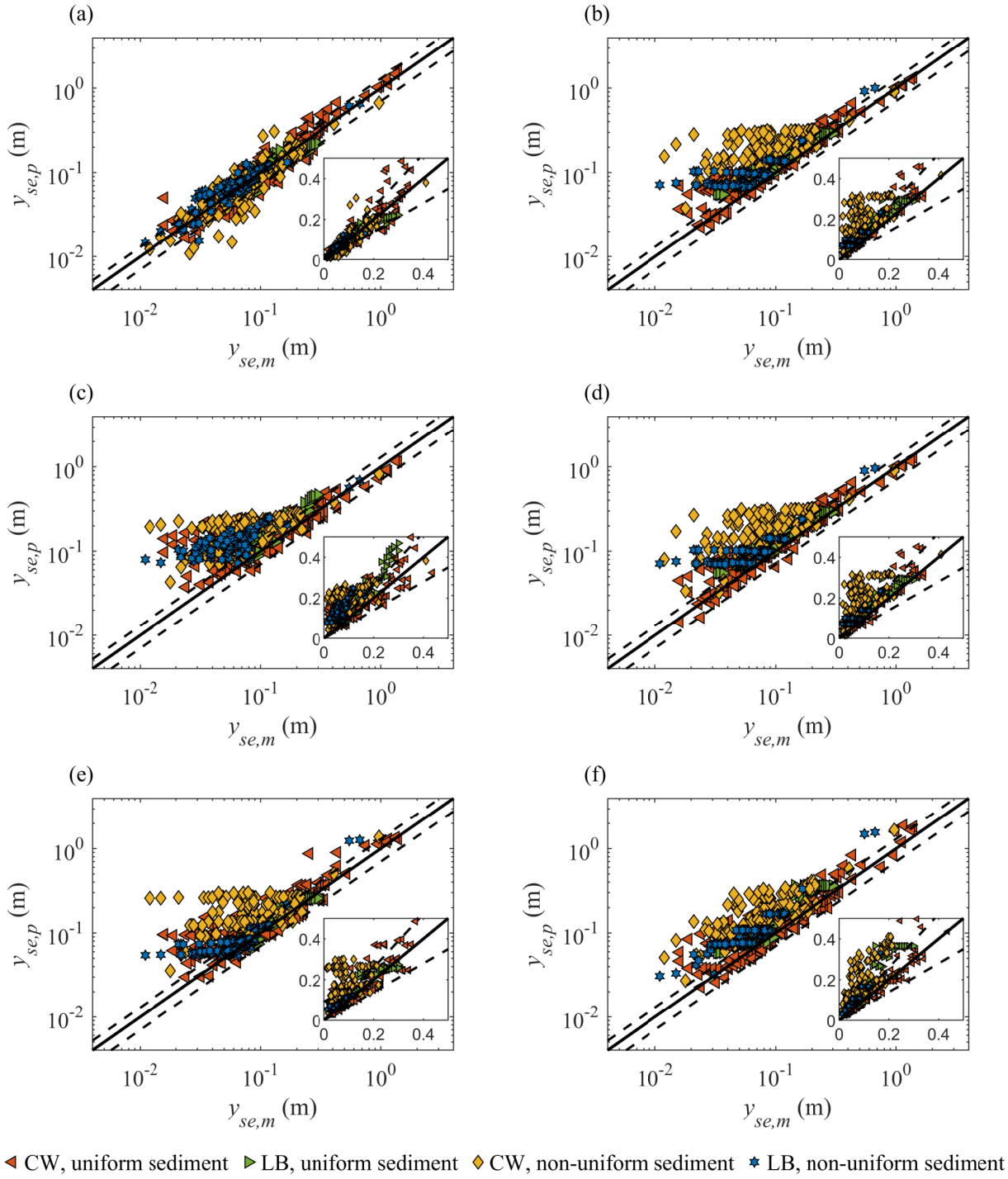

Fig. 4. (a) Measured equilibrium scour depth ($y_{se,m}$) versus predictions ($y_{se,p}$) according to Eqs. (13) and (14); (b) S/M; (c) HEC-18; (d) SM06; (e) F88; and (f) M97. All the data from laboratory experiments reported in Table 1 were used. The solid lines represent a 1:1 agreement, whereas the dashed lines represent the 30% error bounds. In the insets, zoomed-in views of the same graphs are shown in linear coordinates.

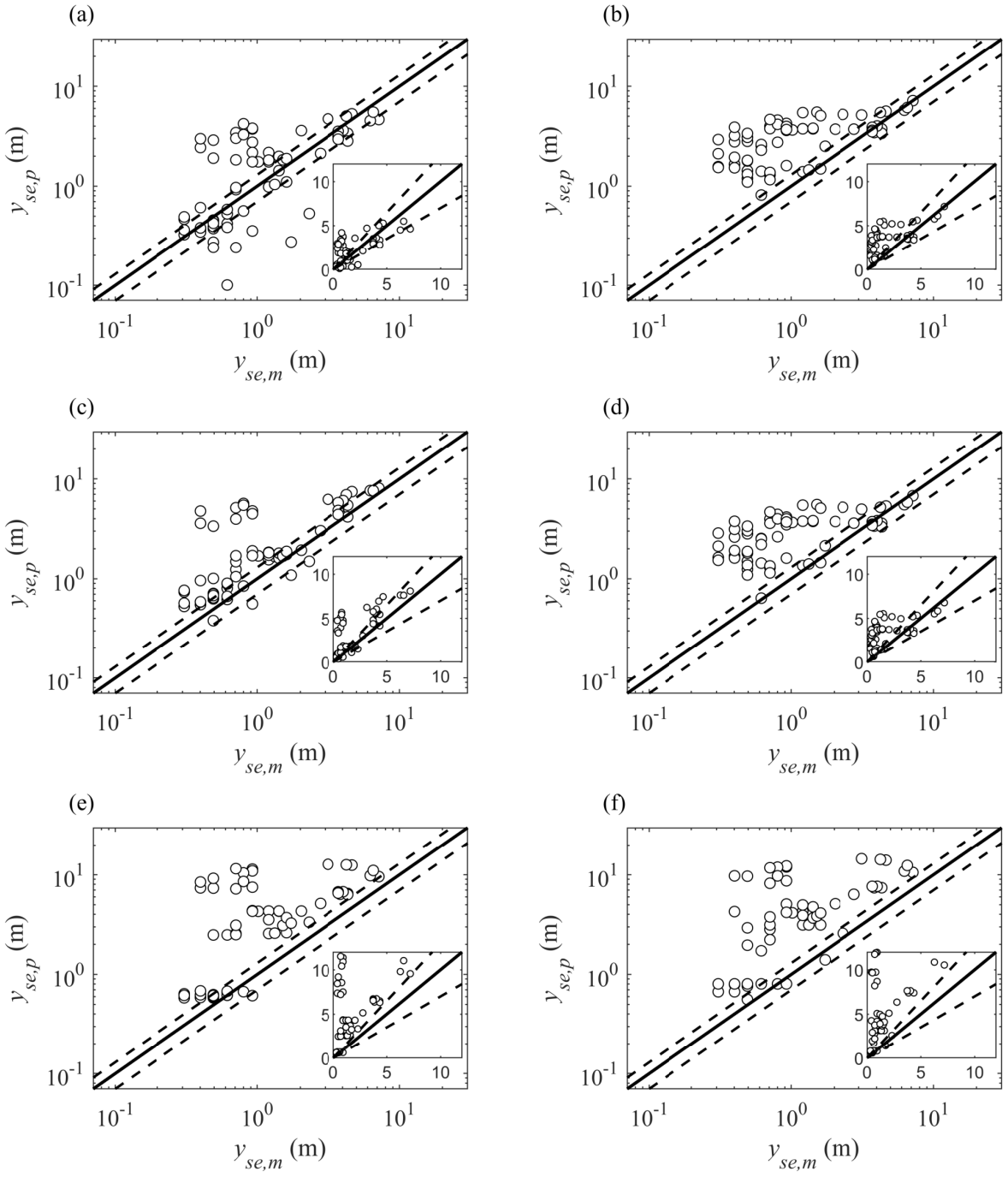

Fig. 5. (a) Measured equilibrium scour depth ($y_{se,m}$) versus predictions ($y_{se,p}$) according to Eqs. (13) and (14); (b) S/M; (c) HEC-18; (d) SM06; (e) F88; and (f) M97. All the data from field measurements reported in Table 1 were used. The solid lines represent a 1:1 agreement, whereas the dashed lines represent the 30% error bounds. In the insets, zoomed-in views of the same graphs are shown in linear coordinates.

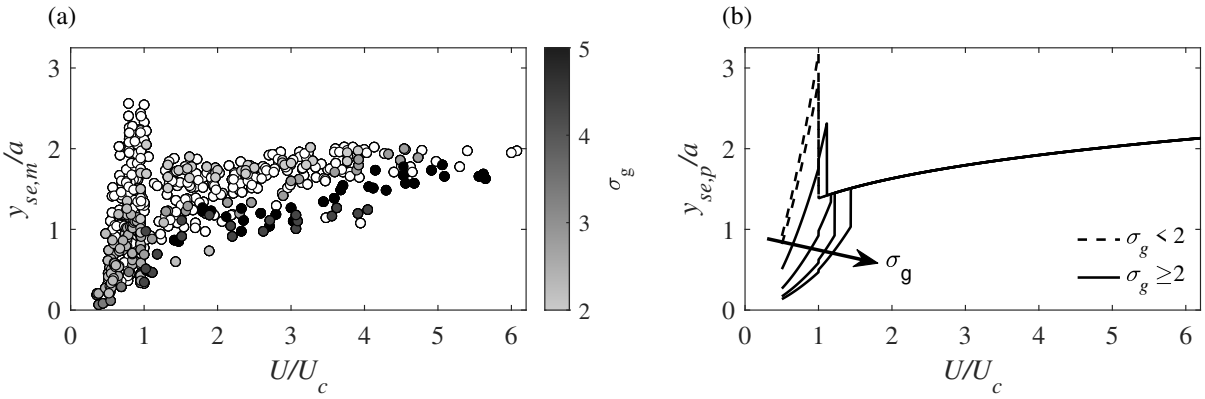

Fig. 6. (a) Normalized measured scour depth of equilibrium $y_{se,m}/a$; and (b) normalized predicted scour depth of equilibrium $y_{se,p}/a$ predicted with Eqs. (13) and (14) versus flow intensity U/U_c. In (a) all the data reported in Table 1 have been used. In (b) we apply Eqs. (13) and (14) to ideal laboratory experiments with $h = 0.25$ m, $a = 0.15$ m, $d_{50} = 2$ mm, $\sigma_g = 1, 1.8, 2.2, 2.5, 2.8, 4.5$ and $U = 0.5U_c - 7U_c$, with U_c calculated from d_{50} as explained in the main text.